AIP | The Journal of Chemical Physics

Local structural effects on orientational relaxation of OH-bond in liquid water over short to intermediate timescales

S. R. Lin, Ping-Han Tang, and Ten-Ming Wu

Citation: The Journal of Chemical Physics **141**, 214505 (2014); doi: 10.1063/1.4902372
View online: http://dx.doi.org/10.1063/1.4902372
View Table of Contents: http://scitation.aip.org/content/aip/journal/jcp/141/21?ver=pdfcov
Published by the AIP Publishing

Local structural effects on orientational relaxation of OH-bond in liquid water over short to intermediate timescales

S. R. Lin, Ping-Han Tang, and Ten-Ming Wu[a)]
Institute of Physics, National Chiao-Tung University, Hsinchu 300, Taiwan

(Received 30 July 2014; accepted 11 November 2014; published online 3 December 2014)

By simulating the rigid simple point charge extended model at temperature $T = 300$ K, the orientational relaxation of the OH-bond in water was investigated over short to intermediate timescales, within which molecules undergo inertial rotation and libration and then enter the rotational diffusion regime. According to the second-cumulant approximation, the orientational time correlation function (TCF) of each axis that is parallel or perpendicular to an OH-bond is related to an effective rotational density of states (DOS), which is determined using the power spectra of angular velocity autocorrelation functions (AVAFs) of the other two axes. In addition, the AVAF power spectrum of an axis was approximated as the rotational stable instantaneous normal mode (INM) spectrum of the axis. As described in a previous study [S. L. Chang, T. M. Wu, and C. Y. Mou, J. Chem. Phys. **121**, 3605 (2004)], simulated molecules were classified into subensembles, according to either the local structures or the H-bond configurations of the molecules. For global molecules and the classified subensembles, the simulation results for the first- and second-rank orientational TCFs were compared with the second-cumulant predictions obtained using the effective rotational DOSs and the rotational stable-INM spectra. On short timescales, the OH-bond in water behaves similar to an inertial rotor and its anisotropy is lower than that of a water molecule. For molecules with three or more H-bonds, the OH-bond orientational TCFs are characterized by a recurrence, which is an indication for libration of the OH-bond. The recurrence can generally be described by the second-cumulant prediction obtained using the rotational stable-INM spectra; however, the orientational TCFs after the recurrence switch to a behavior similar to that predicted using the AVAF power spectra. By contrast, the OH-bond orientational TCFs of molecules initially connected with one or two H-bonds decay monotonically or exhibit a weak recurrence, indicating rapid relaxation into the rotational diffusion regime after the initial Gaussian decay. In addition to accurately describing the Gaussian decay, the second-cumulant predictions formulated using the rotational stable-INM spectra and the AVAF power spectra serve as the upper and lower limits, respectively, for the OH-bond orientational TCFs of these molecules after the Gaussian decay. © *2014 AIP Publishing LLC*. [http://dx.doi.org/10.1063/1.4902372]

I. INTRODUCTION

Water molecules are reoriented in many physical processes, such as proton transport according to the Grotthuss mechanism,[1,2] and in biological systems.[3–5] In water, molecules form a H-bond network and their reorientations are associated with the network reorganization that occurs through the continual breaking and reforming of H-bonds on a timescale of picoseconds. In a sense, the H-bonds connected to each molecule can be considered as an orientational cage that hinders the rotation of the molecule, similar as the cage effect hindering the translational motions of particles in simple liquids.[6,7] Reorganizing the H-bond connection of a molecule releases the molecule from its orientational cage and the reorientation of this molecule involves the rotational diffusion process. For short times, the orientational relaxation of each water molecule is governed by its local structure, which determines the number of H-bonds connected to the molecule and their strengths.

The orientational relaxation of molecular liquids is characterized by the single-molecule orientational time correlation function (TCF), which describes the angular variation of a molecular axis at time t with respect to the initial orientation of the axis. The orientational TCF of molecules in a liquid is defined as

$$C_{\mu}^{(l)}(t) = \langle P_l[\hat{e}_{\mu}(t) \cdot \hat{e}_{\mu}(0)] \rangle, \tag{1}$$

where $\hat{e}_{\mu}$ is a unit vector along the μ direction fixed in the molecular frame, $P_l(x)$ is the Legendre polynomial of order l, and the angular brackets denote the ensemble average over all molecules. For liquid water, the first- and second-rank orientational TCFs, with $l = 1$ and 2, respectively, have been studied using various experimental techniques,[8–10] including dielectric relaxation,[11,12] nuclear magnetic resonance,[13–15] THz absorption spectroscopy,[16,17] the optical-Kerr-effect method,[18] and quasi-elastic neutron scattering.[19,20] These experiments probed the orientational dynamics of water in different molecular-fixed directions (OH-bond, molecular dipole, the line joining two H atoms, and that perpendicular to the molecular plane). The main information obtained is the decay time of the orientational

a)Author to whom correspondence should be addressed. Electronic mail: tmw@faculty.nctu.edu.tw

TCF in the long-time regime and the integrated rotational correlation time, both of which are roughly in the order of picoseconds. In femtosecond IR pump-probe experiments for HOD dissolved in D_2O (H_2O),[8,21–29] the second-rank orientational TCF of the OH (OD) bond has been measured using rotational anisotropy.[30,31] The femtosecond spectroscopy offers several advantages: the timescale of measurements for the orientational TCF is in the order of 100 fs,[27] and the orientational dynamics of OH (OD) bonds connected to H-bonds of different strengths can be extracted by varying the pump and probe frequencies. Thus, the orientational relaxation of HOD subensembles characterized by their local environments was measured using the IR pump-probe technique.[32] These femtosecond experiments have shown that the orientational relaxation of HOD in D_2O at room temperature manifests as two decay processes: a rapid decay process in the first 100 fs and a subsequent slow process with a decay time of approximately 3 ps.[25,26] The orientational relaxation of HOD in D_2O is similar to that of the OH-bond in pure water but the relaxation within 100 fs has yet to be resolved in the IR pump-probe experiments.

The rotational diffusion theory proposed by Debye[33] has frequently been used for describing molecular reorientation in a liquid. In this theory, molecular reorientation in water is assumed to be angular Brownian motion with small-angle steps. Without any memory effect, this theory is valid only for depicting the long-time behavior of orientational TCFs. Moreover, as evidenced by recent simulations[34–38] and experiments,[39–42] molecules in water show large-angle sudden jumps, during which the H-bond partner of an OH-bond of a molecule changes to a third molecule on a timescale of ps. This molecular jump mechanism contradicts the basic assumption of Debye's theory and causes the ratio between the decay times of the first- and second-rank orientational TCFs to be lower than that predicted using the rotational diffusion theory.

To include the memory effect, the generalized Langevin approach has been applied to explain molecular reorientation in dense fluids.[43–50] In this approach, torques experienced by a molecule are separated into rotational resistance with a memory friction kernel contributed from global constituents in the fluid and residual rapid fluctuations that are mostly caused by surrounding molecules. However, the memory friction kernel for molecular reorientation is much more subtle than the orientational TCF to be studied microscopically, and therefore, phenomenological models with fitting parameters have been proposed and used to fit the orientational TCFs of water obtained from experiments or simulations.[48–50] These models provide only a schematic concept for explaining molecular reorientation in water but it is difficult to relate these models to molecular ingredients. In simulations, the memory function for molecular reorientation in water was found to have a long tail extending for approximately 1 ps;[46,47] this complicates the generalized Langevin approach that is used to study molecular reorientation in water.[51]

To describe accurately the short-time behavior of molecular reorientation in liquids, an alternative approach is to trace the orientations of individual molecules by integrating the equations of motion associated with their rotational degrees of freedom as performed in simulations.[52–54] With the evolution of molecular orientations and the ensemble average over molecules, the orientational TCFs of molecular liquids for short times have been formulated using the second-cumulant approximation, which relates the formulas of the orientational TCFs to the angular velocity autocorrelation functions (AVAFs).[55] This approach has been tested for liquids of linear and spherical-top molecules and the principal axes of water molecule. The orientational TCFs calculated by inputting the AVAFs obtained from simulations or based on models were consistent with simulation results on short timescales but showed largely deviations in the long-time limit, as expected.

Over the past two decades, the microscopic dynamics of liquids has been studied from the viewpoint of the potential energy landscape. According to this viewpoint, the instantaneous normal mode (INM) theory of liquids has been developed.[56–58] The TCFs of a liquid on short timescales can be accurately calculated using the INM spectra of the liquid.[59–63] In this study, using the approach of short-time liquid dynamics, we reformulated the oreintational TCFs of water molecules in a coordinate system with three axes either parallel or perpendicular to an OH bond. In the second-cumulant approximation, the formula we obtained for the oreintational TCF of a coordinate axis was associated with the AVAFs of the other two axes. Regarding the power spectra of the AVAFs, our formalism was developed for the frequency domain. We then replaced the AVAF power spectra with the rotational stable-INM spectra of water.[64] There were two advantages in using this stable-INM approximation. First, the OH-bond orientational TCFs of liquid water can be related to the molecular ingredients, without any need for a fitting parameter. Second, we classified water molecules into subensembles according to their local environments and the rotational stable-INM spectra of these subensembles were calculated.[65–67] Using the rotational stable-INM spectra of these subensembles, we could, therefore, examine the local-structure effects on the OH-bond orientational TCFs of water. The second-cumulant predictions, which were calculated using either the AVAF power spectra or the rotational stable-INM spectra, for the OH-bond orientational TCFs were highly consistent with the simulation results on short timescales. In particular, the OH-bond orientational TCFs of molecules with solid-like local structures showed a recurrence that can generally be described by the second-cumulant formulas with the rotational stable-INM spectra as inputs.

The paper is organized as follows: In Sec. II, we present expressions for transformations between the body frame of a water molecule and the OH-bond coordinate system. The orientational TCFs of water molecules in the second- cumulant approximation were formulated in the OH-bond coordinate system. In Sec. III, simulations are summarized and subensembles characterized by local structures are defined. The formalism of the OH-bond orientational TCFs derived in Sec. II is generalized for subensembles. In Sec. IV, simulation results for global molecules and subensembles are presented, and they are compared with the second-cumulant predictions. These comparisons provide insights into the local-structure effect on the orientational relaxation of OH bonds in liquid

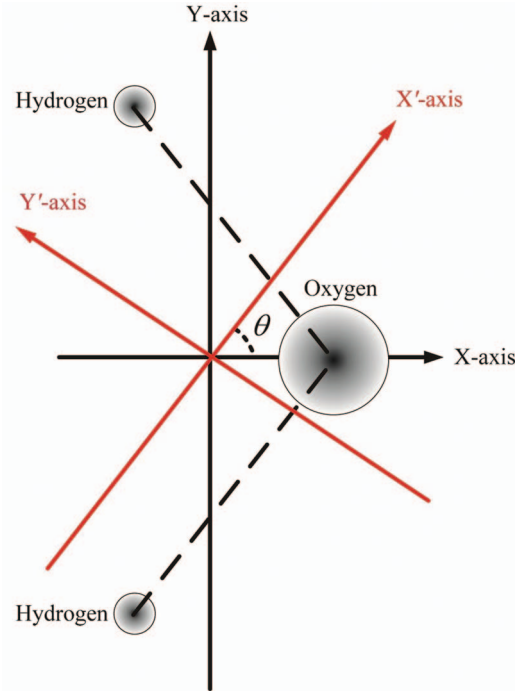

FIG. 1. Body frame of a rigid water molecule. The origin is located at the center of mass of the molecule lying in the x-y plane. The black solid lines are the principal axes of the body frame. The red solid lines are the x' and y' axes that are parallel and perpendicular to an OH bond, respectively. The angle θ equals half the HOH bond angle.

water. Finally, our conclusions and remarks are provided in Sec. V.

II. ORIENTATIONAL TCF

A. Molecular frames and angular velocities

A rigid water molecule consists of two OH bonds of identical length and joined at the O atom to form the HOH bond angle. Fig. 1 shows the body frame of a rigid molecule. The principal x axis passes through the O atom and bisects the HOH bond angle, the y axis is parallel to the line joining two H atoms, and the z axis is perpendicular to the molecular plane. To describe the orientation of an OH bond in a molecule, we used a new coordinate system, in which the x' and y' axes still in the molecular plane are parallel and perpendicular to the OH bond, respectively. As shown in Fig. 1, the new coordinate system can be obtained by rotating the body frame counterclockwise about the z axis through angle θ, which is equal to half the HOH bond angle.

In the body frame, the angular velocity (AV) $\vec{\omega}(t)$ of a water molecule at an instant has three components, $\omega_x(t)$, $\omega_y(t)$, and $\omega_z(t)$, with the instantaneous axes of rotation lying along the principal x, y, and z axis, respectively. In the laboratory (Lab.) frame with the origin fixed at the center of mass, the orientations of the three principal axes change with time, and the AV of a molecule is expressed as

$$\vec{\omega}(t) = \omega_x(t)\hat{e}_x(t) + \omega_y(t)\hat{e}_y(t) + \omega_z(t)\hat{e}_z(t), \qquad (2)$$

where $\hat{e}_j(t)$, in which $j = x, y, z$, is a unit vector in the positive direction of the jth principal axis at time t. In terms of another orthogonal set of unit vectors $\hat{e}_\mu(t)$, where $\mu = \|, \perp, \mathrm{z}$, in the positive direction of the x', y', and z axes, respectively, $\vec{\omega}(t)$ observed in the Lab. frame can be cast into a similar form

$$\vec{\omega}(t) = \omega_{||}(t)\,\hat{e}_{||}(t) + \omega_\perp(t)\,\hat{e}_\perp(t) + \omega_z(t)\,\hat{e}_z(t), \qquad (3)$$

where $\omega_{||}(t)$ and $\omega_\perp(t)$ are components for instantaneous rotations about the x' and y' axes, respectively. Similar to the coordinate transformations between (x', y') and (x, y), $\omega_{||}(t)$, and $\omega_\perp(t)$ are related to $\omega_x(t)$ and $\omega_y(t)$ as follows:

$$\omega_{||}(t) = \omega_x(t)\cos\theta + \omega_y(t)\sin\theta, \qquad (4)$$

$$\omega_\perp(t) = -\omega_x(t)\sin\theta + \omega_y(t)\cos\theta. \qquad (5)$$

In principle, each set of orthonormal vectors can be used to describe the orientation of a rigid water molecule. In the Lab. frame, the evolution of a vector set is governed by the equations[68]

$$\dot{\hat{e}}_\mu(t) \equiv \frac{d\hat{e}_\mu(t)}{dt} = \vec{\omega}(t) \times \hat{e}_\mu(t), \text{ where } \mu = x, y, z \quad \text{or} \quad \mu = ||, \perp, \mathrm{z}, \qquad (6)$$

where $\vec{\omega}(t)$ is given as in Eq. (2) or (3) for the vector set in the (x, y, z) or (x', y', z) system, respectively.

For liquid water in thermal equilibrium, the AV components along the principal axes are considered as stochastic variables and their ensemble averages are zero; in addition, the components along two different axes are statistically independent at any time.[69] Furthermore, the three AV components satisfy the equipartition law. However, the AV components associated with the (x', y', z) axes are somewhat complex. The components $\omega_{||}(t)$ and $\omega_\perp(t)$ are still statistically independent of $\omega_z(t)$ and their ensemble averages vanish. However, these two AV components do not follow the equipartition law since the rotational kinetic energy of a molecule in the (x′, y′, z) system is not simply a sum of harmonic terms. Alternatively, Eqs. (4) and (5) and the equipartition law for the AV components of principal axes can be used to obtain the averages of the squares of $\omega_{||}(t)$ and $\omega_\perp(t)$ as follows:

$$\langle\omega_{||}^2(0)\rangle = \frac{k_B T}{I_x}\cos^2\theta + \frac{k_B T}{I_y}\sin^2\theta, \qquad (7)$$

$$\langle\omega_\perp^2(0)\rangle = \frac{k_B T}{I_x}\sin^2\theta + \frac{k_B T}{I_y}\cos^2\theta, \qquad (8)$$

where k_B is the Boltzmann constant, T is the liquid temperature, and I_j is the moment of inertia with respect to the jth principal molecular axis. Furthermore, $\omega_{||}(t)$ and $\omega_\perp(t)$ are statistically dependent at any instant of time with a non-zero average of their product, because of the finite difference between I_x and I_y for a water molecule.

B. Formalism of the orientational TCFs

We consider the orientational TCFs $C_\mu^{(l)}(t)$ for $\hat{e}_\mu(t)$ in the (x', y', z) system. Although the directions of $\hat{e}_{||}(t)$ and

$\hat{e}_\perp(t)$ pass through the center of mass of a water molecule rather than the O atom, the scalar products $\hat{e}_{||}(t)\cdot\hat{e}_{||}(0)$ and $\hat{e}_\perp(t)\cdot\hat{e}_\perp(0)$ are invariant under any translation or rotation of the coordinate system chosen for evaluating the products. Thus, the anisotropy of OH-bond reorientation in water can be described by the orientational TCFs of the (x′, y′, z) coordinate axes.

By using the approach of short-time liquid dynamics[59–63] and according to the details given in the Appendix, the first-rank orientational TCFs $C_\mu^{(1)}(t)$ along the (x', y', z) axes satisfy the following set of integral equations:

$$C_\mu^{(1)}(t) \approx 1 - \int_0^t (t-\tau)\big(\langle\omega_\eta(\tau)\omega_\eta(0)\rangle C_\nu^{(1)}(\tau) + \langle\omega_\nu(\tau)\omega_\nu(0)\rangle C_\eta^{(1)}(\tau)\big)d\tau, \tag{9}$$

where $\langle\omega_\eta(t)\omega_\eta(0)\rangle$ is the AVAF associated with the ηth axis, and the indices μ, ν, and η ($\mu \neq \nu \neq \eta$) are cyclic in ||, ⊥, and z. The set of integral equations can be solved through iteration, and the solutions for short times are usually determined using a cumulant approximation up to the second order of the AV components.[69] In this cumulant approximation,

$$C_\mu^{(1)}(t) \approx e^{-\psi_\mu(t)}, \tag{10}$$

where

$$\psi_\mu(t) = \int_0^t d\tau(t-\tau)[\langle\omega_\nu(\tau)\omega_\nu(0)\rangle + \langle\omega_\eta(\tau)\omega_\eta(0)\rangle], \quad \text{with } \mu \neq \nu \neq \eta. \tag{11}$$

Based on the derivations provided in the Appendix, the integral equations for the second-rank orientational TCFs are expressed as follows:

$$C_\mu^{(2)}(t) \approx 1 - 3\sum_{\nu\neq\eta\neq\mu}\int_0^t (t-\tau)\langle\omega_\eta(t)\omega_\eta(0)\rangle C_\nu^{(1)}(t)C_\mu^{(1)}(\tau)d\tau. \tag{12}$$

This equation set indicates the hierarchy of the orientational TCFs among different ranks. Similarly, through iteration and by using the second-cumulant approximation, we can break the hierarchy in Eq. (12) and obtain

$$C_\mu^{(2)}(t) \approx e^{-3\psi_\mu(t)}, \tag{13}$$

where $\psi_\mu(t)$ is as given in Eq. (11).

According to the second-cumulant approximation, the formulas for the orientational TCFs in the (x', y', z) system are similar to those for the body frame because of the orthogonality of both coordinate systems.[55] For a coordinate axis, $-\ln C_\mu^{(l)}(t)/l(l+1)$ yields the same function $\psi_\mu(t)$ for different l values in the second-cumulant approximation. This result has been supported by simulations of spherical-top and linear molecules.[52–54] However, the fanning out of $-\ln C_\mu^{(l)}(t)/l(l+1)$ for different l values for long times indicates that the high-order cumulants of an orientational TCF exert a greater effect as time increases. Moreover, while the statistical dependence between $\omega_{||}(t)$ and $\omega_\perp(t)$ has no effect on the second cumulants, it influences the high-order cumulants of an orientational TCF.

C. Effective rotational density of states

The power spectrum of the normalized AVAF $\Omega_\nu(t) \equiv \langle\omega_\nu(t)\omega_\nu(0)\rangle/\langle\omega_\nu^2(0)\rangle$ is given as

$$D_\nu(\omega) = \frac{2}{\pi}\int_0^\infty \Omega_\nu(t)\cos(\omega t)dt, \tag{14}$$

where $D_\nu(\omega)$ is normalized. According to Eqs. (4) and (5), the normalized AVAFs of the x' and y' axes, as well as their power spectra, are related to those of the x and y axes. Using Eqs. (7) and (8), we can express the transformations between the power spectra of the two coordinate systems as

$$D_{||}(\omega) = D_x(\omega)\cos^2\alpha + D_y(\omega)\sin^2\alpha, \tag{15}$$

$$D_\perp(\omega) = D_x(\omega)\sin^2\beta + D_y(\omega)\cos^2\beta, \tag{16}$$

where the transformation angle α for the power spectrum of the x' axis is defined as

$$\cos^2\alpha \equiv \frac{\langle\omega_x^2(0)\rangle}{\langle\omega_{||}^2(0)\rangle}\cos^2\theta = \left[\frac{\cos^2\theta}{I_x} + \frac{\sin^2\theta}{I_y}\right]^{-1}\frac{\cos^2\theta}{I_x}, \tag{17}$$

$$\sin^2\alpha \equiv \frac{\langle\omega_y^2(0)\rangle}{\langle\omega_{||}^2(0)\rangle}\sin^2\theta = \left[\frac{\cos^2\theta}{I_x} + \frac{\sin^2\theta}{I_y}\right]^{-1}\frac{\sin^2\theta}{I_y}. \tag{18}$$

For the power spectrum associated with the y' axis, the angle β is obtained by replacing the subscript || with ⊥ and exchanging x and y in both Eqs. (17) and (18). Thus, α and β are determined by the bond angle of the water molecule and the moments of inertia of the principal x and y axes.

We reformulate $\psi_\mu(t)$ in Eq. (11) in terms of the power spectra of normalized AVAFs,

$$\psi_\mu(t) = \frac{k_B T}{I'_\mu}\int_0^\infty d\omega J_\mu(\omega)\frac{1-\cos(\omega t)}{\omega^2}, \quad \text{with } \mu = ||, \perp, \text{z}, \tag{19}$$

where $I'_{||}$, $I'_\perp$, and I'_z are the effective moments of inertia defined as follows:

$$\frac{1}{I'_{||}} \equiv \frac{\sin^2\theta}{I_x} + \frac{\cos^2\theta}{I_y} + \frac{1}{I_z}, \tag{20}$$

$$\frac{1}{I'_\perp} \equiv \frac{\cos^2\theta}{I_x} + \frac{\sin^2\theta}{I_y} + \frac{1}{I_z}, \tag{21}$$

$$\frac{1}{I'_z} \equiv \frac{1}{I_x} + \frac{1}{I_y}. \tag{22}$$

The effective rotational densities of states are defined as

$$J_{||}(\omega) = I'_{||}\left[\left(\frac{\sin^2\theta}{I_x} + \frac{\cos^2\theta}{I_y}\right)D_\perp(\omega) + \frac{D_z(\omega)}{I_z}\right], \tag{23}$$

$$J_\perp(\omega) = I'_\perp\left[\left(\frac{\cos^2\theta}{I_x} + \frac{\sin^2\theta}{I_y}\right)D_{||}(\omega) + \frac{D_z(\omega)}{I_z}\right], \tag{24}$$

$$J_z(\omega) = I'_z\left(\frac{D_x(\omega)}{I_x} + \frac{D_y(\omega)}{I_y}\right). \tag{25}$$

Notice that $I'_{||}$ and $I'_{\perp}$ are different from the moments of inertia of the water molecule calculated with respect to the x' and y' axes, respectively.[70] For the z axis, which is common to the (x', y', z) and (x, y, z) systems, any one of the two coordinate systems may be used to express $J_z(\omega)$, which is associated with the AVAF power spectra of the other two axes in the chosen system. The expressions for $J_z(\omega)$ in the two systems are related by a transformation. For simplicity, we present the expression of $J_z(\omega)$ in Eq. (25) in the (x, y, z) system.

According to Eq. (19), the function of $\psi_\mu(t)$, and therefore, the orientational TCFs of the μ axis are completely determined by$J_\mu(\omega)$; this is the main theme of this paper. We refer to $J_\mu(\omega)$ as the effective rotational density of states (DOS) along the μ axis, and it contains information on the OH-bond reorientation associated with this axis. As indicated by Eqs. (23)–(25), the effective rotational DOS along a coordinate axis in an orthogonal system is associated with the AVAF power spectra of the other two axes. In Subsection II D, we show that the effective rotational DOSs of a system can be related to the molecular ingredients of the system by using the INM approach.

D. Stable-INM approximation

For almost two decades, the short-time dynamics of liquids has been studied using the INM theory,[59–63] which has facilitated obtaining valuable results.[71–75] An essential feature of this theory is the INM spectrum, which is the ensemble average of the eigenmodes of mass-weighted Hessian matrices over liquid configurations. The INM spectrum of water has been studied using several models. The INM spectrum of rigid water molecules in liquid phases can be separated into translational and rotational components by using projectors defined by the INM eigenvectors.[64] For liquid water, the rotational INM spectra associated with the principal axes, denoted as $D_\nu^{INM}(\omega)$, where $\nu = x, y, z$, can be calculated using a standard procedure.[65]

Since the inertial tensor of a molecule in a coordinate system other than its body frame is not diagonal, it is difficult to construct mass-weighted Hessian matrices of liquid water in the (x', y', z) system. A simple method is to relate the rotational INM spectra evaluated in the (x', y', z) system to those associated with the principal axes by using coordinate transformations. In the INM theory, in which particle dynamics of a liquid is considered harmonic, the power spectrum of a normalized AVAF along an axis is generally reduced to the rotational INM spectrum of the axis.[59,64] Therefore, similar to Eqs. (15) and (16), the rotational INM spectra of the x' and y' axes, denoted as $D_{||}^{INM}(\omega)$ and $D_{\perp}^{INM}(\omega)$, respectively, can be obtained as follows:

$$D_{||}^{INM}(\omega) \equiv D_x^{INM}(\omega)\cos^2\alpha + D_y^{INM}(\omega)\sin^2\alpha, \quad (26)$$

$$D_{\perp}^{INM}(\omega) \equiv D_x^{INM}(\omega)\sin^2\beta + D_y^{INM}(\omega)\cos^2\beta. \quad (27)$$

In the stable-INM approximation, in which the imaginary branch of the INM spectrum is neglected, the AVAF power spectrum $D_\nu(\omega)$ is further approximated as the rotational stable-INM spectrum $D_\nu^{INM,s}(\omega)$, which is renormalized.[59,76,77] Normally, the lower the fraction of imaginary INMs in a system is, the more accurate the stable-INM approximation. Low fractions of imaginary INMs are found in systems at low temperatures or those with H-bonds, such as liquid water.[64,78] Similarly, Eqs. (26) and (27) are suitable for the rotational stable-INM spectra of the two coordinate systems. Hence, in the stable-INM approximation, the effective rotational DOSs in the (x', y', z) system are related to the rotational stable-INM spectra of the principal axes according to the matrix equation

$$\begin{bmatrix} J_{||}^{INM,s}(\omega) \\ J_{\perp}^{INM,s}(\omega) \\ J_z^{INM,s}(\omega) \end{bmatrix} = \begin{bmatrix} \frac{I'_{||}\sin^2\theta}{I_x}, & \frac{I'_{||}\cos^2\theta}{I_y}, & \frac{I'_{||}}{I_z} \\ \frac{I'_{\perp}\cos^2\theta}{I_x}, & \frac{I'_{\perp}\sin^2\theta}{I_y}, & \frac{I'_{\perp}}{I_z} \\ \frac{I'_z}{I_x}, & \frac{I'_z}{I_y}, & 0 \end{bmatrix} \begin{bmatrix} D_x^{INM,s}(\omega) \\ D_y^{INM,s}(\omega) \\ D_z^{INM,s}(\omega) \end{bmatrix}. \quad (28)$$

The $\psi_\mu(t)$ function in the stable-INM approximation is calculated by using Eq. (19) with the approximate effective rotational DOSs in this matrix equation as the inputs. After $\psi_\mu(t)$ is obtained, $C_\mu^{(1)}(t)$ and $C_\mu^{(2)}(t)$ are evaluated by using Eqs. (10) and (13), respectively.

III. MODEL, SIMULATION, AND SUBENSEMBLE

We performed MD simulations with a time step of 1 fs for 256 SPC/E water molecules confined in a cubic box and at thermodynamic conditions with density $\rho = 1$ g/cm^3 and temperature $T = 300$ K; the details on our simulations are presented in Ref. 65. Water molecules with randomly distributed velocities were initially positioned at fcc lattice sites. We neglected the first 300 ps to enable the simulated system to reach equilibrium, and subsequently, we collected data on 10^6 configurations at every one step.

As in Ref. 65, the structures of the simulated liquids were analyzed using two methods: Voronoi tessellation[79] and H-bond configuration. As in our previous studies,[65–67] the molecules in a configuration were classified into either four Voronoi groups (VGs) according to the asphericity of the Voronoi polyhedron associated with each molecule[80] or ten H-bond configurations. In each type of classification, a subensemble consisted of molecules belonging to a VG or with the same H-bond configuration. The selector $\Theta_j(\xi)$ of molecule j was set as one if the molecule belonged to a subensemble indexed with ξ; otherwise, the selector was set as zero.

To investigate the influence of local environments on the orientational dynamics of molecules, we defined the orientational TCFs of subensemble ξ as

$$C_{\mu\xi}^{(l)}(t) = \left\langle \frac{1}{N_\xi}\sum_{j=1}^{N} P_l[\hat{e}_{j\mu}(t)\cdot\hat{e}_{j\mu}(0)]\Theta_\xi(j)\right\rangle, \quad (29)$$

where $\hat{e}_{j\mu}(t)$ is a unit vector parallel to the μ axis of molecule j at time t, and N_ξ is the number of molecules belonging to the subensemble in a liquid containing a total of N molecules. The normalized AVAF $\Omega_{\mu\xi}(t)$ of molecules in subensmble ξ was defined similarly, and its power spectrum $D_{\mu\xi}(\omega)$ was obtained using Eq. (14). The effective rotational DOSs of

this subensemble for different axes were evaluated using Eq. (23)–(25) and the AVAF power spectra of the subensemble. Therefore, the orientational TCFs of a subensemble were calculated in a manner similar to that used for global molecules. All calculations in the stable-INM approximation were generalized for the classified subensembles.[65]

IV. RESULTS AND DISCUSSION

For the SPC/E water molecule, the OH bond length is 1 Å and the HOH bond angle (2θ) is 109.47°, with $\cos^2\theta \approx 1/3$ and $\sin^2\theta \approx 2/3$. Among the principal moments of inertia, I_y is the smallest and I_z is the largest, with $I_z = I_x + I_y$ for a plane molecule.[65] The effective moments of inertia $I'_{||}$, $I'_{\perp}$, and I'_z obtained from Eqs. (20)–(22) were 1.050, 0.877, and 0.681 $\times 10^{-40}$ g-cm^2, respectively. The transformation angles α and β calculated by using Eq. (17) were 64.8° and 43.3°, respectively, with their sum being close to the HOH bond angle.

A. Global molecules

The normalized AVAFs $\Omega_v(t)$ along the x', y', and z-axes and their power spectra $D_v(\omega)$ are shown in Fig. 2. Using the AVAF power spectra of the x' and y' axes and those of the principal x and y axes (not shown), we show that the transformations in Eqs. (15) and (16) are satisfied. According to these transformations, the contribution to $D_{||}(\omega)$ was mostly from the power spectra of the principal y axis, while that to $D_{\perp}(\omega)$ was equally from the power spectra of the x and y axes.[81] Thus, $D_{||}(\omega)$ and $D_{\perp}(\omega)$ had somewhat different spectral shapes, even though both had a width (FWHM) of approximately 570 cm^{-1}. $D_{||}(\omega)$ had a maximum at 710 cm^{-1}, whereas $D_{\perp}(\omega)$ had a maximum at 510 cm^{-1} and a shoulder near 900 cm^{-1}. Both of these spectra were broader than $D_z(\omega)$, which had a maximum near 510 cm^{-1} and a width of 330 cm^{-1}.

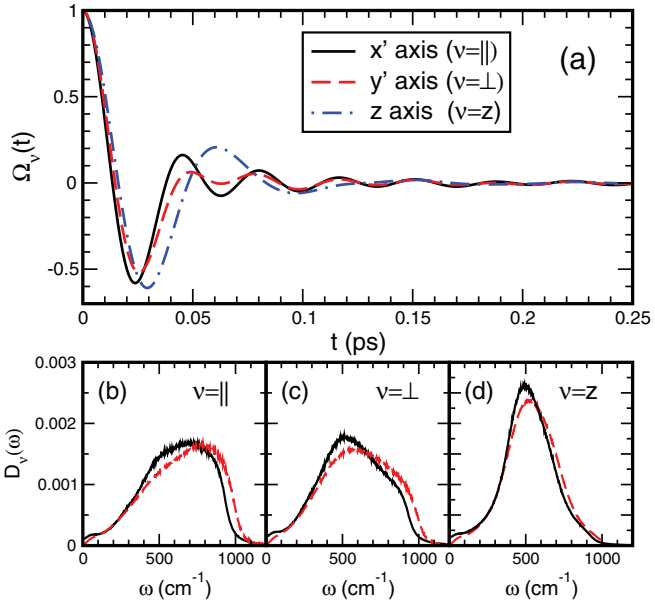

FIG. 2. (a) Normalized AVAFs of the SPC/E model at $T = 300$ K and $\rho = 1$ g/cm^3. The solid, dashed, and dotted-dashed lines are the simulation results for the x', y', and z axes, respectively. The lower panels (b), (c), and (d) show the comparison between the AVAF power spectra (black solid lines) and the rotational stable-INM spectra (red dashed lines) for the x', y', and z axes, respectively.

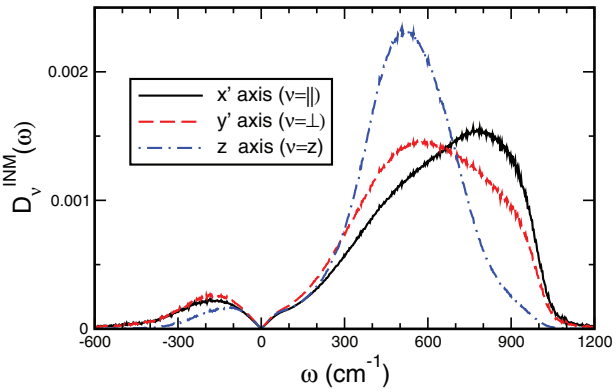

FIG. 3. Rotational INM spectra. The solid, dashed, and dotted-dashed lines are for the x', y', and z axes, respectively. Each spectrum is normalized.

The normalized rotational INM spectra of the principal axes were re-calculated with a resolution higher than those reported in Ref. 65, and the corresponding spectra of the x' and y' axes were obtained using Eqs. (26) and (27), respectively. The rotational INM spectra along the x', y', and z axes are shown in Fig. 3 and their unstable fractions $\tilde{f}_\mu$ were estimated to be 6.8%, 7.5%, and 3.7%, respectively.[65] After neglecting the unstable branch and a renormalization for the stable branch, the rotational stable-INM spectra of the three axes are shown in Figs. 2(b)–2(d). Compared with the AVAF power spectrum, the rotational stable-INM spectrum of each axis extended toward high frequencies, with the position of the spectral maximum being blue shifted and the spectral width being broadened.[82]

Fig. 4 shows the effective rotational DOS $J_{||}(\omega)$, $J_{\perp}(\omega)$, and $J_z(\omega)$ along the x', y', and z axes, respectively; their stable-INM approximations and the contributions of the three principal axes are also shown. The common features of the three effective DOSs were that the spectral maximum was essentially contributed from the principal x and z axes, while the shoulder on the high-frequency side contained contributions mainly from the y-axis. The maxima of $J_{||}(\omega)$, $J_{\perp}(\omega)$, and $J_z(\omega)$ were located at $\omega_m \approx 500$, 530, and 600 cm^{-1} and their spectral widths were approximately 450, 560, and 600 cm^{-1}, respectively. The stable-INM approximation led to the effective rotational DOS showing a moderate extension at the high-frequency end such that the maximum frequencies $\omega_m^{INM,s}$ of $J_{||}^{INM,s}(\omega)$, $J_{\perp}^{INM,s}(\omega)$, and $J_z^{INM,s}(\omega)$ were near 540, 600, and 760 cm^{-1}, respectively, and their spectral widths were approximately 520, 620, and 650 cm^{-1}, respectively. For each axis, the essential difference between $J_\mu(\omega)$ and $J_\mu^{INM,s}(\omega)$ lay in their low-frequency behaviors. Calculated using the AVAF power spectra, $J_\mu(\omega)$ had a non-zero value at $\omega = 0$. This zero-frequency value was proportional to the rotational diffusion coefficient,[6] which determined the relaxation times of the orientational TCFs associated with the axis. However, as shown in Fig. 4, $J_\mu^{INM,s}(\omega)$ was linearly extrapolated to zero at $\omega = 0$, similar to the ohmic spectral function of quantum dissipative systems.[83–86] The low-frequency behavior of

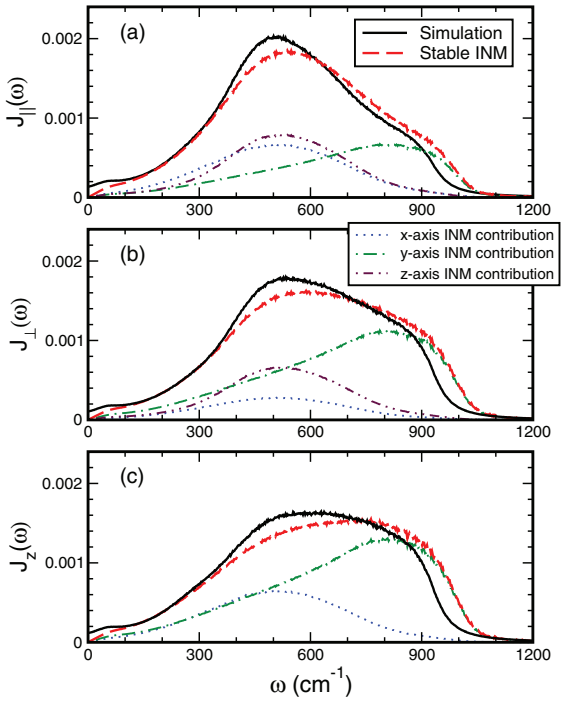

FIG. 4. Effective rotational DOSs of the SPC/E model: (a) for x' axis, (b) for y' axis, and (c) for z axis. The black solid lines are the results calculated using the power spectra of normalized AVAFs generated by simulations, and the red dashed lines are the results calculated using the rotational stable-INM spectra. In each panel, the stable-INM approximation is separated into contributions from the principal x, y, and z axes, indicated using the dotted, dotted-dashed, and dotted-dotted-dashed lines, respectively.

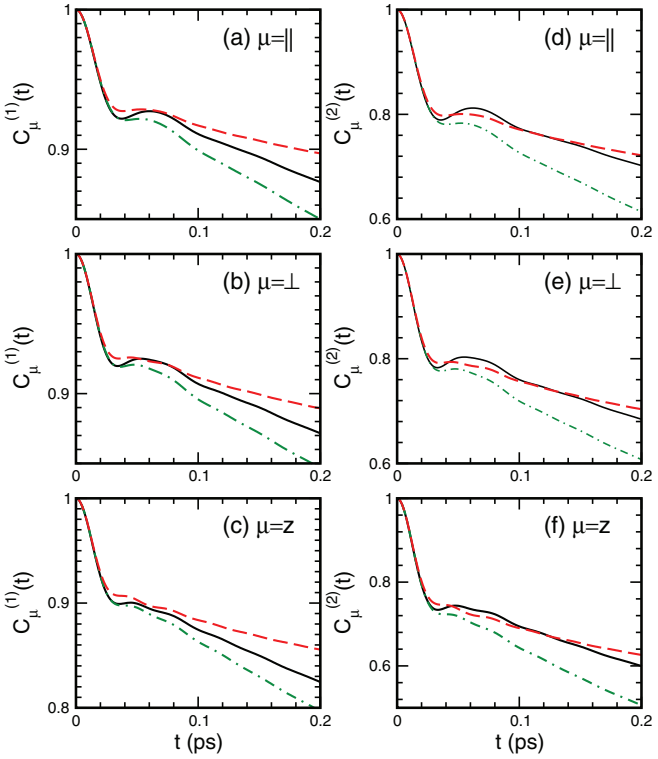

FIG. 5. Orientational TCFs of the first-rank (left column) and the second-rank (right column) calculated for SPC/E liquid water at $T = 300$ K and $\rho = 1$ g/cm^3: (a) and (d) for x' axis, (b) and (e) for y' axis, and (c) and (f) for z axis. The solid lines are the simulation results. The dotted-dashed and dashed lines are the results of the second-cumulant predictions evaluated using the effective rotational DOSs and their stable-INM approximations shown in Fig. 4, respectively.

$J_\mu^{INM,s}(\omega)$ is attributed to the fact that the stable rotational INMs do not cause orientational diffusion of molecules. Consequently, the long-time behavior of the orientational TCF predicted by $J_\mu^{INM,s}(\omega)$ was quite different from that predicted by$J_\mu(\omega)$. We discuss this in Sec. IV B.

The first- and second-rank orientational TCFs along the x', y', and z axes were obtained from simulations and by using the second-cumulant approximation, and they are shown in Fig. 5 for times preceding 0.2 ps. Clearly, as evidenced by the good agreement between the results obtained using the two methods, the orientational TCFs along any axis initially follow a Gaussian decay given by

$$C_\mu^{(l)}(t) \approx \exp\left[-\frac{1}{2}\left(\frac{t}{\tau_\mu^{(l)}}\right)^2\right], \quad \text{with } \mu = ||, \perp, \text{z}, \quad (30)$$

where the decay time is expressed as

$$\tau_\mu^{(l)} = \left(\frac{2I'_\mu}{l\,(l+1)\,k_B T}\right)^{1/2}. \quad (31)$$

For $T = 300$ K and $l = 1$, $\tau_\mu^{(l)}$, where $\mu = \|, \perp, z$, is estimated to be 0.071, 0.065, and 0.053 ps, respectively. Hence, within a time of approximately 0.02 ps, an OH bond in liquid water at $T = 300$ K behaves as a free rotor with three moments of inertia, denoted by I'_μ ($\mu = \|, \perp, z$), and therefore, the anisotropy of the rotor is lower compared with that of a water molecule.[87] Consequently, the Gaussian decay of the orientational TCFs results from the thermal average for the inertial rotations of the OH-bonds in water.

As indicated by the simulation results, the orientational TCFs along the x', y′, and z axes deviated from the Gaussian decay as time increased and reached a minimum at t_{min}, which was near 0.033–0.037 ps for $l = 1, 2$. After the minimum, the orientational TCFs for $l = 1, 2$ showed a maximum; however, the recurrence depended on the orientational axis of the TCF. The maxima in the first- and second-rank orientational TCFs along an axis occurred almost at the same time t_{max}, which was near 0.060, 0.054, and 0.046 ps for the x', y', and z axes, respectively. We defined the recurrence amplitude of an orientational TCF as the difference between the maximum and minimum values of the TCF at t_{max} and t_{min}, respectively. We found that for each axis the recurrence amplitude for $l = 1$ was smaller than that for $l = 2$. For each l, the recurrence amplitudes associated with the x' and y' axes were close in magnitude; however, the amplitude associated with the z axis was relatively smaller. The recurrence is usually considered to be caused by under-damped librational motions resulting from hindrance by neighbors of a molecule.[9] After the recurrence, all orientational TCFs generally decayed monotonically; however, small deviations from the monotonic behavior were observed in the TCFs along the z axis.

As shown in Fig. 5 for the x', y', and z axes, the second-cumulant predictions obtained using the effective rotational DOSs were highly consistent with the simulation results

for the orientational TCF before t_{min}; however, the deviation of the predictions increased with time. By contrast, the second-cumulant predictions obtained using the stable INMs were in complete agreement with the simulation results only over timescales shorter than t_{min}; this was consistent with past observations for other TCFs predicted using the stable INMs.[77,88,89] However, although not in complete agreement with the simulation results, in general, the predictions obtained using the stable INMs for the orientational TCFs captured the behavior of the simulation results up to approximately 0.1 ps; during this period, the recurrence was included.

According to Eq. (19), we interpreted the decay of $C_\mu^{(l)}(t)$ as resulting from the dephasing of rotational normal modes with the effective DOS $J_\mu^{INM,s}(\omega)$. Some features of the recurrence in $C_\mu^{(l)}(t)$, if any, could be related to the effective DOS. The values of t_{min} and t_{max} were roughly estimated using $2\pi/\omega_c^{INM,s}$ and $2\pi/\omega_m^{INM,s}$, respectively, where $\omega_c^{INM,s}$ was the cutoff frequency of the effective DOS, and the recurrence amplitude was associated with the spectral width of the effective DOS. Additional discussion of subensembles is provided in Subsection IV B.

B. Local-structure effect

In this subsection, we discuss the investigation of the structural effects on OH-bond reorientation in liquid water by examining the orientational TCFs along the x' and y' axes for subensembles with different local-structure features. The results for the z axis were similar to those for the x' and y' axes.

1. Subensembles of VGs

By dividing the asphericity (η) distribution of the SPC/E liquid into four regions, with the partitions set at $\eta = 1.46$, 1.72, and 1.98, we classified water molecules in each liquid configuration into four subensembles, indexed from VG I to VG IV in the order of increasing η value.[65–67,80] On average, VG II contained the majority of molecules, with a molecular fraction close to two thirds, and had a lifetime longer than 1 ps; the VG lifetime was estimated as the decay of the TCF of the VG index to one half.[65] VG III had a molecular fraction of approximately 30% and a lifetime near 0.24 ps. VG I and IV each had a molecular fraction of 1.5% and their lifetimes were estimated to be 60 and 45 fs, respectively. In VG IV, approximately 70% of the molecules had four nearest neighbors in tetrahedral-like arrangements. The nearest neighbors of molecules in VG I were randomly distributed and gave rise to a plateau in the O-atom radial distribution function at distances near the first minimum of the corresponding distributions of the other three VGs. In the H-bond network, most molecules in VG IV had four H-bonds; however, the number of H-bonds connected to molecules in VG I varied, with one donated H-bond and one accepted H-bond being the most probable case.

In the upper two panels in Fig. 6, we present the normalized rotational INM spectra of the x' and y' axes for the four VGs. From VG I to VG IV, the stable INM branches of the two axes shifted toward high frequencies and the fractions of unstable INMs decreased; these results are consistent with the trend observed regarding the principal axes.[65] However, some

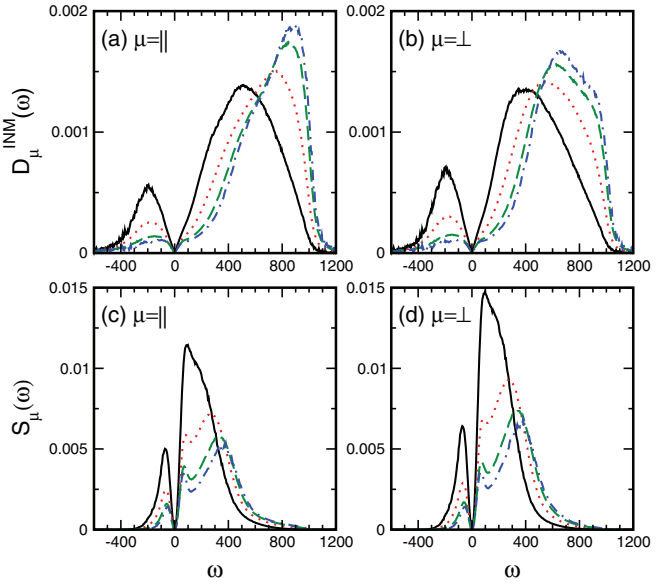

FIG. 6. Normalized rotational INM spectrum (upper panels) and the product of normalized rotational and translational INM spectra (lower panels) for a VG. The left and right columns are for the x' and y' axes, respectively. The solid, dotted, dashed, and dotted-dashed lines are for VG I–VG IV, respectively. In (c) and (d), the ordinates for the product have been multiplied by a factor of 10^4.

features specific to the x' and y' axes were evident: For the x' axis, a hump emerged on the low-frequency side of the maximum in the stable branch as the η value increased. By contrast, for the y' axes, a shoulder grew on the high-frequency side of the maximum. These features were attributed to the rotational INM spectra of the x' and y' axes, which are given by Eqs. (26) and (27), respectively, having different relative contributions from the principal x and y axes.

In Fig. 7, we present the effective rotational DOSs of the four VGs calculated for the x' axis; the stable-INM approximations of the DOSs are also shown for comparison.

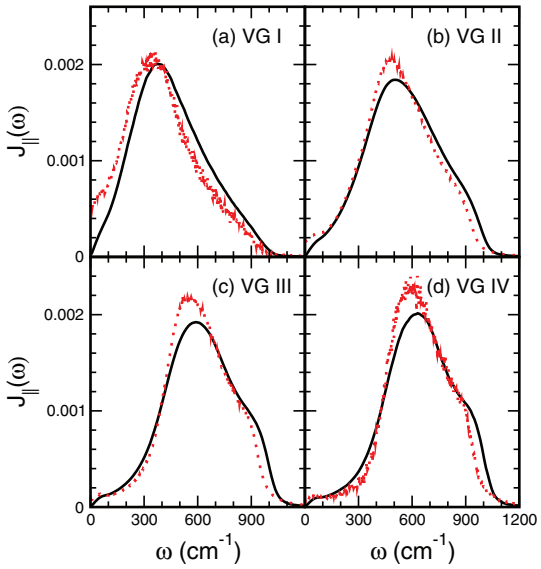

FIG. 7. Effective rotational DOS along the x' axis for molecules in a VG. Panels (a)–(d) are for VG I–VG IV, respectively. The red-dotted and black-solid lines are the results calculated using the AVAF power spectra and the rotational stable-INM spectra, respectively.

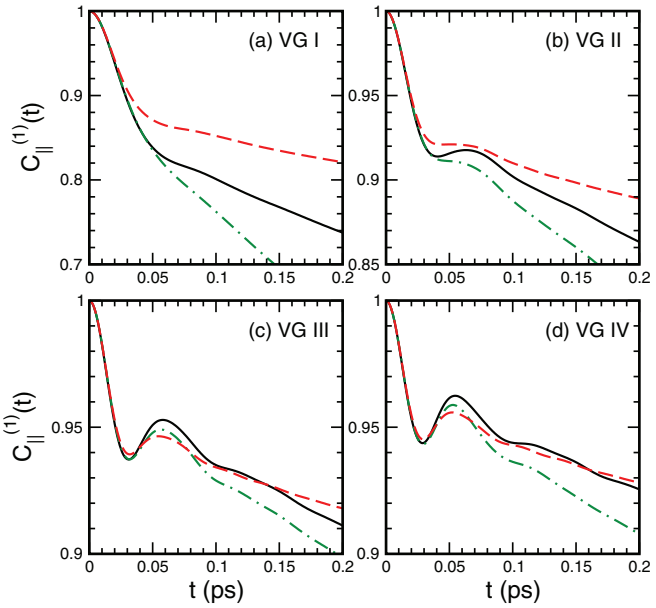

FIG. 8. The first-rank orientational TCF along the x' axis for molecules in a VG: (a) VG I, (b) VG II, (c) VG III, and (d) VG IV. The line indications are the same as those in Fig. 5.

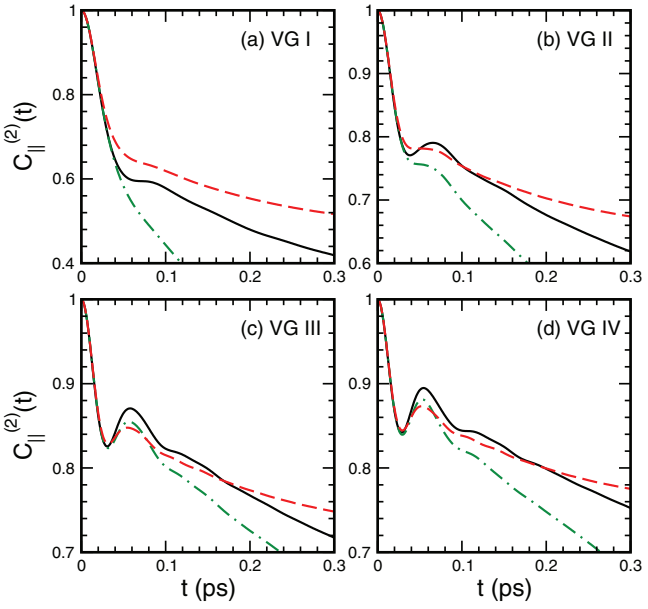

FIG. 9. Same as Fig. 8 except for the second-rank orientational TCF along the x' axis.

The DOSs calculated for the y'-axis were similar in behavior to those obtained for the x' axis. As shown in Fig. 7, the effective rotational DOSs of the four VGs had different shapes. The DOS of VG I showed a maximum near 340 cm^{-1}, a width of approximately 400 cm^{-1}, and a high-frequency tail. The DOSs of VG II, III, and IV were roughly equal in width (approximately 430 cm^{-1}), but showed maxima near 480, 560, and 590 cm^{-1}, respectively. Thus, from VG I to VG IV, the high-frequency tail in the DOS was shortened and a shoulder appeared in the region. At zero frequency, the DOS of VG I had the largest value among the DOSs of the four subensembles, and the DOS of VG IV had the smallest value, with the two extreme values differing by an order of magnitude. Therefore, molecules in VG I were expected to have a large rotational diffusion coefficient,[6] while those in VG IV were expected to have a small rotational diffusion coefficient. As in the case of global molecules, the stable-INM approximation caused the maximum position in the effective rotational DOS of VG I and that of VG IV to blueshift by approximately 20 and 40 cm^{-1}, respectively, and increased the spectral widths of the DOSs by 40–90 cm^{-1} from VG I to VG IV.

The orientational TCFs along the x' axis for the four VGs are shown in Figs. 8 and 9 for $l = 1$ and $l = 2$, respectively; the TCFs were calculated using simulations and the second-cumulant prediction. The initial Gaussian decay in the orientational TCF of each rank was verified using the cumulant formula, and it was found to be the same for the four VGs. However, after the Gaussian decay, the orientational TCFs of the four VGs behaved differently. For VG I, no recurrence occurred in the orientational TCFs for $l = 1$, 2, although a plateau near 0.06–0.08 ps was observed in the curve of $l = 2$. Such a monotonic decay of the orientational TCF indicated that torques experienced by molecules in VG I were too weak to cause substantial librations before their orientational motions relaxed into the rotational diffusion regime. This fast orientational relaxation was manifested by two features of the rotational INM spectrum of VG I: a large fraction of unstable rotational INMs and a significant overlap in the stable lobe between the rotational and translational INM spectra, which is shown in the lower panels in Fig. 6. In this study, we defined the overlap as

$$S_{\mu\xi}(\omega) = D_{\mu\xi}^{INM}(\omega) \cdot D_{T\xi}^{INM}(\omega), \tag{32}$$

where $D_{T\xi}^{INM}(\omega)$ is the normalized translational INM spectrum of VG ξ. For water, the stable lobe of $D_{T\xi}^{INM}(\omega)$ roughly covers frequencies lower than 400 cm^{-1}.[65] The first feature indicates that molecules in VG I can follow a large number of possible paths to surmount potential energy barriers and to give rise to rotational diffusion. The second feature suggests that, the orientational cages of molecules in VG I are formed by weak H-bonds and broken by the coupling between the rotational and translational motions of the molecules. The breaking of the cage leads to the rapid OH-bond orientational relaxation, resulting in the molecules in VG I entering the rotational diffusion regime early. Because of the rapid orientational relaxation, the second-cumulant prediction for the OH-bond orientational TCFs of VG I calculated using either the AVAF power spectra or the rotational stable INMs are accurate only up to the initial Gaussian decay timescale.

For VG II–VG IV, a recurrence was observed in the first- and second-rank orientational TCFs and small variations followed the recurrence for VG III and VG IV. The recurrence amplitude increased with the asphericity of local structures. The appearance of a recurrence could be understood by considering the case of VG IV. As shown in Fig. 6, the tetrahedral-like local structures of molecules in VG IV yielded only a small fraction of unstable modes in the rotational INM spectrum. Since the available paths for crossing over energy barriers are scarce, these molecules

generally rotate in confined potential energy wells, exhibiting librational motions. Furthermore, as shown in Figs. 6(c) and 6(d), the stable-branch overlap $S_{\mu\xi}(\omega)$ of VG IV was the smallest among the four VGs, indicating weak coupling between rotational and translational motions for molecules in VG IV. Therefore, the orientational cages of these molecules, which are mostly connected by four H-bonds, are difficult to break, and therefore, molecular librations within these cages persist for some time. Consequently, a recurrence manifested in their orientational TCFs, and small variations followed the recurrence. These results indicate that the OH-bond reorientation of molecules in VG IV was delayed to enter the rotational diffusion regime.

Figs. 8 and 9 show that, as in the case of global molecules, the second-cumulant predictions obtained using the effective rotational DOSs of the four VGs were in strong agreement with the simulation results before t_{min}, but manifested increasing deviations after the minimum. However, the second-cumulant predictions obtained using the stable INMs generally captured the behavior of recurrence and the subsequent variations observed in the first- and second-rank TCFs of VG III and VG IV; moreover, the prediction timescale was prolonged. These results indicate that the prediction timescale obtained using the stable INMs for the orientational TCFs increased with the asphericity of molecular local structures. The reason is that molecules with large asphericity values have solid-like local structures, which favor the stable-INM approach, while molecules with small asphericity values have liquid-like local structures, which limit the applicability of the stable-INM theory.

2. Subensembles of H-bond configurations

We further investigated the relationship between OH-bond reorientation and H-bond configurations of molecules, focusing on the orientational TCFs at times after the recurrence. The H-bond was defined using the energetic criterion presented in Ref. 65. Two molecules connected by an H-bond are referred to a donor and an acceptor for they donate and accept the intermediate proton of the H-bond, respectively. For a molecule donating k and accepting m H-bonds, we denote its H-bond configuration as DkAm.

For the SPC/E liquid, there were a total of ten possible H-bond configurations in our simulated liquids. The molecular fractions and the lifetimes of these configurations have been presented in Ref. 65, where the lifetimes were estimated in a manner similar to that used for the VG lifetimes. With a molecular fraction close to 40%, D2A2 was the most probable configuration and had a lifetime of approximately 166 fs. With a total fraction near 40%, D2A1 and D1A2 had lifetimes near 20 and 13 fs, respectively. Among configurations with two H-bonds, D1A1 had a lifetime of 11 fs and a molecular fraction near 12%, while D2A0 and D0A2 had a total molecular fraction of 2% and each survived for a few femtoseconds. The rest of the molecules belonged to configurations with one or five H-bonds, and they had lifetimes shorter than 10 fs. Examples of D2A3 and D3A2 are shown in Figs. 10(a) and 10(b), respectively. In D3A2, the triplet molecules

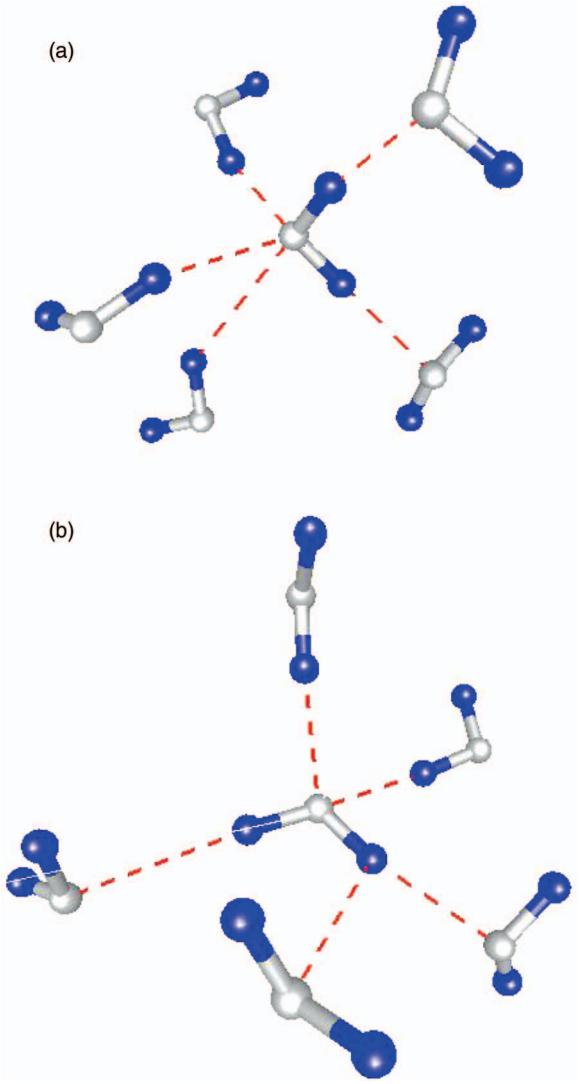

FIG. 10. Configurations with five H-bonds: (a) D2A3 and (b) D3A2. Each configuration is composed of six molecules, which were generated using the simulated liquid. The white and blue circles stand for the O and H atoms, respectively. The red-dashed lines indicate the H-bond.

connected with two H-bonds sharing the same proton act similarly as the transition state of the jump reorientation mechanism.[10,34,36]

In Fig. 11, we present the normalized rotational stable-INM spectra of the x' and y' axes calculated for the ten H-bond configurations; the results for the same n_D are plotted in one panel. We assigned n_D and n_A as the numbers of donated and accepted H-bonds in a H-bond configuration, respectively. For each axis, the rotational stable-INM spectrum of a H-bond configuration showed strong dependence on the n_D value since the spectral shape shifts toward higher frequencies as n_D increases. Quantitatively, the spectral shift of the rotational stable-INM spectrum of a subensemble can be determined according to its average frequency $\omega_{\mu\xi}$.[90] In Fig. 12, the average frequencies of the ten H-bond configurations are plotted against $n = n_D + n_A$ for the x' and y' axes, with the manner of plotting being similar to that presented in Ref. 67 for the intramolecular INM bands of flexible SPC/E water model. For each axis, $\omega_{\mu\xi}$ linearly increased

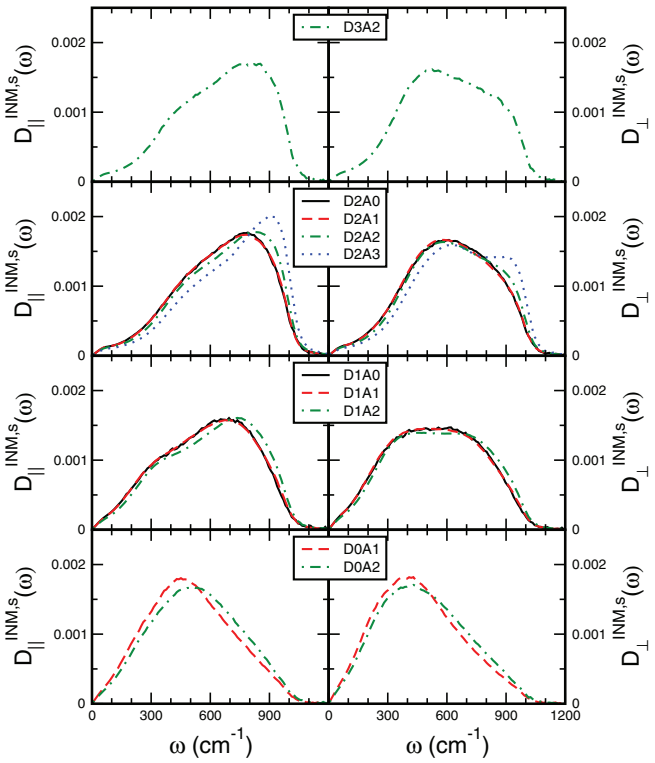

FIG. 11. Normalized rotational stable-INM spectra for ten H-bond configurations. The left and right columns are the results for the x' and y' axes, respectively. In each column, the panels from top to bottom are the results for H-bond configurations with three, two, one, and zero donated H-bonds. In all panels, the solid, dashed, dotted-dashed, and dotted lines indicate the results for H-bond configurations with zero, one, two, and three accepted H-bonds, respectively.

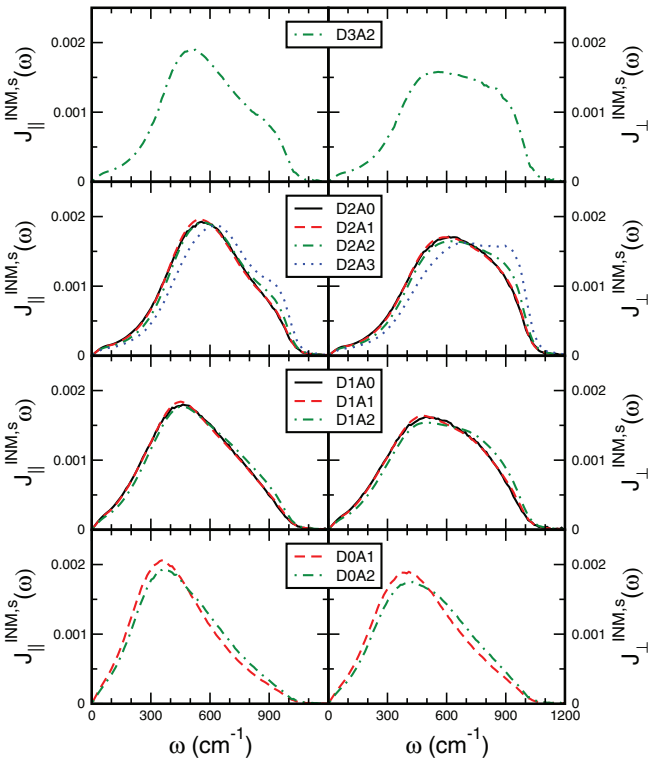

FIG. 13. Same as Fig. 11 except for the effective rotational DOSs in the stable-INM approximation.

with n_D when n was lower than four. Averaged for the linear lines fit to each data set with the same n_A, the mean slope S_D for the linear increase of $\omega_{\mu\xi}$ with n_D was approximately 75 and 72 cm^{-1} for the x' and y' axes, respectively. In Fig. 12, $\omega_{\mu\xi}$ linearly increased with n_A (shown by the dashed lines); however, the slope S_A of this linearity was smaller than S_D and showed dependence on n_D. This result differs from the slope S_A for the intramolecular INM bands.[67] For molecules

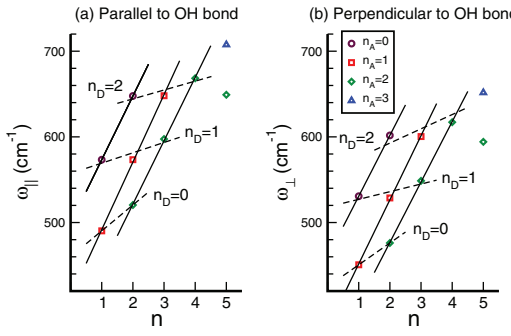

FIG. 12. Average rotational INM frequency versus the number n of H-bonds in a configuration: (a) the x' axis and (b) the y' axis. In each panel, circles, squares, diamonds, and triangles are for H-bond configurations with zero, one, two, and three accepted H-bonds, respectively. The solid lines are the linear curves fit to each data set of the same number of accepted H-bond. The dashed lines from top to bottom are the linear curves fit to data sets of two, one, and zero donated H-bonds, respectively.

with only accepted H-bonds (the dashed lines for $n_D = 0$ in Fig. 12), S_A was roughly 30 and 25 cm^{-1} for the x' and y' axes, respectively. This indicated that the shift of the rotational stable-INM spectrum caused by molecules with only accepted H-bonds was approximately one half to one third of that caused by molecules with donated H-bonds. However, for molecules with donated H-bonds (the dashed lines for $n_D = 1$ or $n_D = 2$ in Fig. 12), the effect of the accepted H-bonds on $\omega_{\mu\xi}$ was markedly suppressed, with S_A reduced to approximately 15 and 10 cm^{-1} for the x' and y' axes, respectively. According to our analysis, the donated H-bonds play a dominant role in OH-bond reorientation in liquid water, as in the case of molecular reorientation about the principal axes.[65] Relative to the data of D2A2, $\omega_{\mu\xi}$ of molecules with five H-bonds may increase or decrease, depending on whether the fifth H-bond is an accepted or donated bond, respectively.

In Fig. 13, we present the effective rotational DOS in the stable-INM approximation, $J_{\mu}^{INM,s}(\omega)$, calculated for the ten H-bond configurations. Similar to the results for the four VGs shown in Fig. 7, the stable-INM approximation caused the effective rotational DOS of each H-bond configuration to shift moderately toward high frequencies. Apparently, the effective rotational DOS was strongly influenced by the donated H-bonds of a molecule and weakly by the accepted H-bonds. As shown in Fig. 13, a high-frequency shoulder emerged as the total number of H-bonds connected to a molecule increased. Relative to D2A2, the fifth H-bond in D2A3 lengthened the blueshift, while the fifth H-bond in D3A2 shortened the spectral shift.

For the ten H-bond configurations, the first- and second-rank orientational TCFs of the x' axis are shown on a

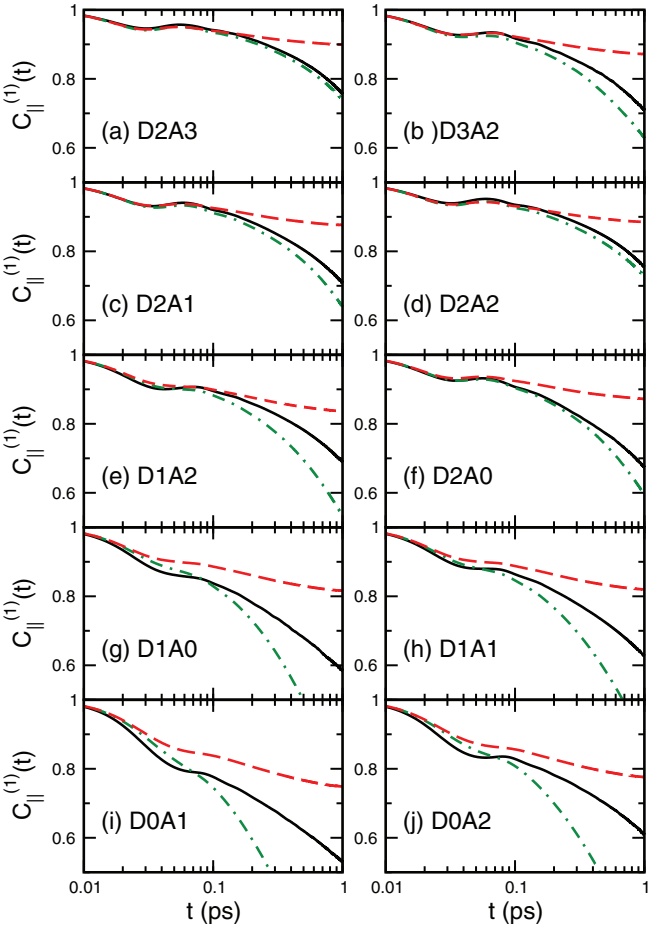

FIG. 14. The first-rank orientational TCFs along the x' axis calculated for the indicated H-bond configurations. In each panel, the abscissa is plotted in logarithmic time scale and the line indications are the same as those in Fig. 5.

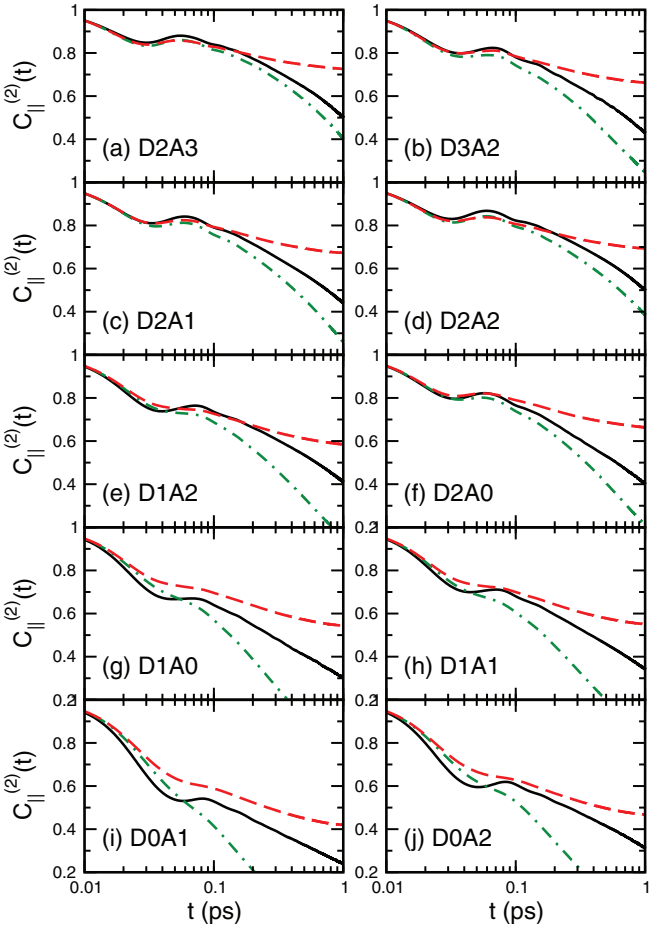

FIG. 15. Same as Fig. 14 except for the second-rank orientational TCFs along the x' axis.

logarithmic timescale in Figs. 14 and 15, respectively, for the time duration 0.01–1 ps. The TCFs for the y′ axis were similar in behavior to those for the x′-axis. Here, we focus on the behavior of the orientational TCF from 0.1 to 1 ps. In liquid water, molecular reorientation on this timescale generally changes from librational motions to rotational diffusion and can be determined using the ultrafast IR spectroscopy,[9,27] which was described in Introduction. Observations from Figs. 14 and 15 are described as follows: First, the timescale for making an accurate prediction by using the second-cumulant approximation was associated with the H-bond configuration determined at initial, generally varying with the total number of H-bonds of a configuration. Second, in the time window between 0.1 and 1 ps, the second-cumulant prediction obtained using the effective rotational DOS of each H-bond configuration behaved differently from that obtained using the stable INMs, with the two different predictions serving as the upper and lower limits for the orientational TCF obtained from simulations. We describe the two limiting behaviors as follows.

Because of its linearity at low frequencies, $J_{\mu}^{INM,s}(\omega)$ behaves as an ohmic spectral density. The $\psi_{\mu}(t)$ function expressed in Eq. (19) was analyzed by using the method for dissipative quantum systems with an ohmic spectral function presented in Refs. 85 and 86. The $\psi_{\mu}(t)$ function calculated using the stable INMs was observed to diverge logarithmically in time; for long times, this divergence led to a power-law decay in the orientational TCF. However, the asymptote of $\psi_{\mu}(t)$ evaluated using the effective rotational DOS, which has a finite value at zero frequency, exhibited a linear increase with time, causing the orientational TCF to decay exponentially in the long-time limit. Thus, the overall behavior of the orientational TCF predicted using the stable INMs changed from a Gaussian to a power-law decay, whereas the prediction obtained using the effective rotational DOS indicated changes from a Gaussian to an exponential decay, with the former close to a straight line and the later resembling as a convex curve on a logarithmic timescale from 0.1 to 1 ps (Figs. 14 and 15).

For configurations with at least three H-bonds, the simulation results of the orientational TCFs, for $l = 1, 2$, generally were consistent with the predictions obtained using the stable INMs during the recurrence and immediately after the maximum, but the behavior of the TCFs changed toward those predicted using the effective rotational DOSs after the recurrence. Particular attention must be given to D2A3 molecules, because minor differences between the simulation results and the predictions were observed between 0.1 and 1 ps. The prediction times for the orientational TCFs were generally

longer than the lifetimes of these H-bond configurations, indicating that the memory for OH-bond reorientation of these molecules was longer than the lifetimes of their H-bond configurations. A physical picture is provided as follows: For molecules initially connected with three or more H-bonds, their orientational cages are stiff and delay their reorientation relaxations into the rotation diffusion regime by breaking and reforming H-bonds, which have already changed their initial H-bond connections. Once the molecules leave their H-bond cages, the reorientation of these molecules relax and their orientational TCFs decay in exponential characteristics.

For configurations with one or two H-bonds with lifetimes less than 10 fs, the orientational TCFs exhibited weak or no recurrence. Generally, the predictions obtained using the effective rotational DOSs deviated from the simulation results after the initial Gaussian decay, except that the weak recurrence in the second-rank orientational TCF of D2A0 molecules was in agreement with the prediction. The deviation occurred on a timescale close to the lifetime of the H-bond configuration and increased with time, indicating that the OH-bond reorientation causes these molecules to lose the memory of their initial H-bond configurations. In addition, we notice that for molecules having only one H-bond initially, such as D0A1 and D1A0, the orientational TCFs from 0.1 to 1 ps were close to a linear curve as shown in Figs. 14 and 15. According to our results, the orientational cages of these molecules, which are connected with only one or two H-bonds, are weak and place little restriction on their orientations, leading to these molecules entering the rotational diffusion regime on the timescales of the lifetimes of their initial H-bond configurations.

V. CONCLUSIONS

In this study, we investigated OH-bond reorientation in liquid water over short to intermediated time scales. This phenomenon has recently been studied using femtosecond IR measurements. Using the SPC/E water model, we calculated the first- and second-rank orientational TCFs along three axes that were parallel or perpendicular to an OH bond of a water molecule. In the second-cumulant approximation, the orientational TCFs along each axis in this coordinate system were determined using an effective rotational DOS that was related to the power spectra of AVAFs associated with the other two axes. We further approximated the AVAF power spectrum of an axis with the rotational stable-INM spectrum of the axis, which could be evaluated using the molecular ingredients of the system. Simulation results for the orientational TCFs were compared with the second-cumulant predictions obtained using either the power spectra of the AVAFs generated by simulations or the rotational stable-INM spectra, without any need for a fitting parameter.

On timescales shorter than 0.01 ps, the OH bond in water, which is characterized by the Gaussian decay of the orientational TCFs, behaves as an inertial rotor with anisotropy lower than that of a water molecule. After the Gaussian decay and within 0.1 ps, a recurrence manifests in the orientational TCFs of all axes. To date, recurrences have not been observed experimentally, and they are usually interpreted as arising from under-damped librational motions of molecules because of hindrance by their neighbors. According to our analyses, the recurrence can alternatively be attributed to the dephasing of rotational stable INMs. The recurrence is associated with the rotational axis of OH-bond reorientation and strongly depends on local structures of water molecules.

We define the recurrence amplitude as the difference between the maximum and minimum values of an orientaitonal TCF after the initial Gaussian decay. The recurrence amplitude increases with the asphericity of molecular local structures. A large recurrence amplitude is associated with tetrahedral-like local structures of molecules that are connected mainly with three or four H-bonds; small variations subsequent to the recurrence are observed in the orientational TCFs of these molecules. These molecules are confined within orientational cages well connected by H-bonds and perform librational motions for some time. Thus, the librational motions of these molecules delay the OH-bond reorientation to enter the rotational diffusion regime. The recurrence in their orientational TCFs can generally be described by the second-cumulant prediction obtained using the rotational stable-INM spectra. After the recurrence, the orientational TCFs of these molecules change behavior to that predicted by using the AVAF power spectra.

Molecules initially connected with one or two H-bonds have local structures with low asphericity. The orientational cages of these molecules weakly restrict molecular orientations, and therefore, their OH-bond orientational TCFs decay monotonically or show a weak recurrence. The INM spectra of these molecules are characterized by a large fraction of unstable rotational INMs, and the rotational and translational INM spectra in the stable branch have a substantial overlap. All of these regarding the INM spectrum support that the OH-bond reorientation of these molecules relaxes into the rotational diffusion regime after the initial Gaussian decay of their orientational TCFs. The Gaussian decay was clearly described by the second-cumulant prediction obtained using the rotational stable-INM spectra or the AVAF power spectra. According to our results, the two cumulant predictions serve as the upper and lower limits for the OH-bond orientational TCFs of these molecules after the Gaussian decay.

ACKNOWLEDGMENTS

This work is supported by National Science Council, Taiwan under Grant No. NSC 102-2112-M-009-013-MY3.

APPENDIX: INTEGRAL EQUATIONS FOR THE FIRST- AND SECOND-RANK ORIENTATIONAL TCFs

In terms of the initial condition $C_\mu^{(1)}(0) = 1$, the approach of short-time liquid dynamics[60,62] provides

$$C_\mu^{(1)}(t) = 1 + \int_0^t (t-\tau)\ddot{C}_\mu^{(1)}(\tau)d\tau, \quad \text{with } \mu = ||, \perp, \text{z}, \tag{A1}$$

where the second time derivative of $C_\mu^{(1)}(t)$ is expressed as

$$\ddot{C}_\mu^{(1)}(t) = \langle \ddot{\hat{e}}_\mu(t) \cdot \hat{e}_\mu(0)\rangle = -\langle \dot{\hat{e}}_\mu(t) \cdot \dot{\hat{e}}_\mu(0)\rangle. \tag{A2}$$

The second equality in Eq. (A2) is due to the integration by part for the TCF of a system at thermal equilibrium.[47] By using Eq. (6) in the text for $\dot{\hat{e}}_\mu(t)$ and $\dot{\hat{e}}_\mu(0)$ individually in (A2), we have

$$\ddot{C}_\mu^{(1)}(t) = -\sum_{\nu,\eta}\sum_{\sigma,\rho}\varepsilon_{\mu\nu\eta}\varepsilon_{\mu\sigma\rho}\langle\omega_\eta(t)\omega_\rho(0)\rangle\langle\hat{e}_\nu(t)\cdot\hat{e}_\sigma(0)\rangle, \tag{A3}$$

where $\varepsilon_{\mu\nu\eta}$ is the Levi-Civita symbol with subscript indices in ∥, ⊥, z. The statistical independence between unit vectors and the AV components has been assumed. For small times, the direction of $\hat{e}_\nu(t)$ is not deviated too much from its initial direction, so that $\hat{e}_\nu(t)$ is almost orthogonal to the other two unit vectors at $t = 0$. Thus, we have the approximation

$$\langle\hat{e}_\nu(t)\cdot\hat{e}_\sigma(0)\rangle \approx \delta_{\nu\sigma}C_\nu^{(1)}(t), \tag{A4}$$

where $\delta_{\nu\sigma}$ is the Kronecker delta. Hence, Eq. (A3) can be simplified as

$$\ddot{C}_\mu^{(1)}(t) \approx -\sum_{\nu\neq\eta\neq\mu}\langle\omega_\eta(t)\omega_\eta(0)\rangle C_\nu^{(1)}(t). \tag{A5}$$

After substituting the approximated $\ddot{C}_\mu^{(1)}(t)$ into Eq. (A1), we have Eq. (9) in the text.

For $l = 2$, $C_\mu^{(2)}(t) \equiv \langle[3(\hat{e}_\mu(t)\cdot\hat{e}_\mu(0))^2 - 1]/2\rangle$ satisfies an equation similar as Eq. (A1), except for replacing $\ddot{C}_\mu^{(1)}(t)$ with the second time derivative of $C_\mu^{(2)}(t)$, which is expressed as the follow:

$$\ddot{C}_\mu^{(2)}(t) = 3\langle(\dot{\hat{e}}_\mu(t)\cdot\hat{e}_\mu(0))^2\rangle + 3\langle(\hat{e}_\mu(t)\cdot\hat{e}_\mu(0))(\ddot{\hat{e}}_\mu(t)\cdot\hat{e}_\mu(0))\rangle. \tag{A6}$$

By using Eq. (6) for $\dot{\hat{e}}_\mu(t)$, the first term in Eq. (A6) is vanished because of the orthogonality between $\dot{\hat{e}}_\mu(t)$ and $\hat{e}_\mu(0)$ for small times. By using an integration by part for the second term in Eq. (A6), we have

$$\begin{aligned}\ddot{C}_\mu^{(2)}(t) = &-3\langle(\dot{\hat{e}}_\mu(t)\cdot\hat{e}_\mu(0))^2\rangle \\ &-3\langle(\hat{e}_\mu(\mathrm{t})\cdot\dot{\hat{e}}_\mu(0))(\dot{\hat{e}}_\mu(t)\cdot\hat{e}_\mu(0))\rangle \\ &-3\langle(\hat{e}_\mu(t)\cdot\hat{e}_\mu(0))(\dot{\hat{e}}_\mu(t)\cdot\dot{\hat{e}}_\mu(0))\rangle.\end{aligned} \tag{A7}$$

The first two terms in Eq. (A7) are vanished due to the same reason given above and the third term is factorized into a product of two TCFs. Therefore, we have

$$\ddot{C}_\mu^{(2)}(t) \approx 3C_\mu^{(1)}(t)\ddot{C}_\mu^{(1)}(t). \tag{A8}$$

By Eq. (A5),

$$\ddot{C}_\mu^{(2)}(t) \approx -3C_\mu^{(1)}(t)\sum_{\nu\neq\eta\neq\mu}\langle\omega_\eta(t)\omega_\eta(0)\rangle C_\nu^{(1)}(t). \tag{A9}$$

After substituting $\ddot{C}_\mu^{(2)}(t)$ in Eq. (A9) into the integral equation for $C_\mu^{(2)}(t)$, we obtain Eq. (12) in the text.

[1] N. Agmon, Chem. Phys. Lett. **244**, 456 (1995).
[2] M. Bonn, H. J. Bakker, G. Rago, F. Pouzy, J. R. Siekierzycka, A. M. Brouwer, and D. Bonn, J. Am. Chem. Soc. **131**, 17070 (2009).
[3] R. Pomès and B. Roux, Biophy. J. **71**, 19 (1996).
[4] F. Despa, A. Fernández, and R. S. Berry, Phys. Rev. Lett. **93**, 228104 (2004).
[5] F. Despa and R. S. Berry, Biophy. J. **92**, 373 (2007).
[6] M. G. Mazza, N. Giovambattista, F. W. Starr, and H. E. Stanley, Phys. Rev. Lett. **96**, 057803 (2006).
[7] M. G. Mazza, N. Giovambattista, H. E. Stanley, and F. W. Starr, Phys. Rev. E **76**, 031203 (2007).
[8] K. J. Tielrooij, C. Petersen, Y. L. A. Rezus, and H. J. Bakker, Chem. Phys. Lett. **471**, 71 (2009).
[9] H. J. Bakker and J. L. Skinner, Chem. Rev. **110**, 1498 (2010), and references therein.
[10] D. Laage and J. T. Hynes, in *Ultrafast Infrared Vibrational Spectroscopy*, edited by M. D. Fayer (CRC Press, New York, 2013).
[11] R. Buchner, J. Barthel, and J. Stauber, Chem. Phys. Lett. **306**, 57 (1999).
[12] J. Barthel, K. Bachhuber, R. Buchner, and H. Hetzenauer, Chem. Phys. Lett. **165**, 369 (1990).
[13] J. R. C. van der Maarel, D. Lankhorst, J. de Bleijser, and J. C. Leyte, Chem. Phys. Lett. **122**, 541 (1985).
[14] J. Ropp, C. Lawrence, T. C. Farrar, and J. L. Skinner, J. Am. Chem. Soc. **123**, 8047 (2001).
[15] E. H. Hardy, A. Zygar, M. D. Zeidler, M. Holz, and F. D. Sacher, J. Chem. Phys. **114**, 3174 (2001).
[16] C. Rønne, L. Thrane, P. O. Åstrand, A. Wallqvist, K. V. Mikkelsen, and S. R. Keiding, J. Chem. Phys. **107**, 5319 (1997).
[17] C. Rønne and S. R. Keiding, J. Mol. Liq. **101**, 199 (2002).
[18] K. Winkler, J. Lindner, H. Bürsing, and P. Vöhringer, J. Chem. Phys. **113**, 4674 (2000).
[19] J. Teixeira, M. C. Bellissent-Funnel, S. H. Chen, and A. J. Dianoux, Phys. Rev. A **31**, 1913 (1985).
[20] A. Faraone, L. Liu, C. Y. Mou, P. C. Shih, J. R. D. Copley, and S. H. Chen, J. Chem. Phys. **119**, 3963 (2003).
[21] S. Woutersen, U. Emmerichs, and H. J. Bakker, Science **278**, 658 (1997).
[22] H. J. Bakker, S. Woutersen, and U. Emmerichs, Chem. Phys. **258**, 233 (2000).
[23] H. K. Nienhuys, R. A. van Santen, and H. J. Bakker, J. Chem. Phys. **112**, 8487 (2000).
[24] G. Gallot, S. Bratos, S. Pommeret, N. Lascoux, J.-Cl. Leicknam, M. Koziński, W. Amir, and G. M. Gale, J. Chem. Phys. **117**, 11301 (2002).
[25] J. J. Loparo, C. J. Fecko, J. D. Evaes, S. T. Roberts, and A. Tokmakoff, Phys. Rev. B **70**, 180201 (2004).
[26] C. J. Fecko, J. J. Loparo, S. T. Roberts, and A. Tokmakoff, J. Chem. Phys. **122**, 054506 (2005).
[27] D. E. Moilanen, E. E. Fenn, Y. S. Lin, J. L. Skinner, B. Bagchi, and M. D. Fayer, Proc. Natl. Acad. Sci. U.S.A. **105**, 5295 (2008).
[28] H. J. Bakker, Y. L. A. Rezus, and R. L. A. Timmer, J. Phys. Chem. A **112**, 11523 (2008).
[29] R. A. Nicodemus, S. A. Corcelli, J. L. Skinner, and A. Tokmakoff, J. Phys. Chem. B **115**, 5604 (2011).
[30] T. Tao, Biopolymer **8**, 609 (1969).
[31] G. Lipari and A. Sxabo, Biophys. J. **30**, 489 (1980).
[32] C. P. Lawrence and J. L. Skinner, J. Chem. Phys. **118**, 264 (2003).
[33] P. Debye, *Polar Molecules* (Chem. Cat., New York, 1929).
[34] D. Laage and J. T. Hynes, Science **311**, 832 (2006).
[35] D. Laage and J. T. Hynes, Chem. Phys. Lett. **433**, 80 (2006).
[36] D. Laage and J. T. Hynes, J. Phys. Chem. B **112**, 14230 (2008).
[37] D. Laage, G. Stirnemann, F. Sterpone, R. Rey, and J. T. Hynes, Annu. Rev. Phys. Chem. **62**, 395 (2011).
[38] D. Laage, G. Stirnemann, F. Sterpone, and J. T. Hynes, Acc. Chem. Res. **45**, 53 (2012).
[39] J. D. Eaves, J. J. Loparo, C. J. Fecko, S. T. Roberts, A. Tokmakoff, and P. L. Geissler, Proc. Natl. Acad. Sci. U.S.A. **102**, 13019 (2005).
[40] D. E. Moilanen, D. Wong, D. E. Rosenfeld, E. E. Fenn, and M. D. Fayer, Proc. Natl. Acad. Sci. U.S.A. **106**, 375 (2009).
[41] S. Park, M. Odelius, and K. J. Gaffney, J. Phys. Chem. B **113**, 7825 (2009).
[42] M. Ji, M. Odelius, and K. J. Gaffney, Science **328**, 1003 (2010).
[43] W. A. Steele, in *Molecular Liquids, Dynamics and Interactions*, edited by A. J. Barnes, W. J. Orville-Thomas, and J. Yarwood (Reidel, Dordrecht, 1984).
[44] B. J. Gertner and K. Lindenberg, J. Chem. Phys. **94**, 5143 (1991).
[45] A. P. Blokhin and M. F. Gelin, J. Phys. Chem. B **101**, 236 (1997).
[46] T. Yamaguchi, S. H. Chong, and F. Hirata, J. Chem. Phys. **116**, 2502 (2002).
[47] T. Yamaguchi, and F. Hirata, J. Chem. Phys. **117**, 2216 (2002).
[48] A. G. St. Pierre and W. A. Steele, Phys. Rev. A **184**, 172 (1969).
[49] M. F. Gelin and D. S. Kosov, J. Chem. Phys. **124**, 144514 (2006).
[50] M. F. Gelin and D. S. Kosov, J. Chem. Phys. **130**, 134502 (2009).
[51] J. P. Hanson and I. R. McDonald, *Theory of Simple Liquids*, 2nd ed. (Academic Press, London, 1986).
[52] R. M. Lynden-Bell and I. R. McDonald, Mol. Phys. **43**, 1429 (1981).

[53]R. M. Lynden-Bell, in *Molecular Liquids, Dynamics and Interactions*, edited by A. J. Barnes, W. J. Orville-Thomas, and J. Yarwood (Reidel, Dordrecht, 1984).
[54]R. M. Lynden-Bell and W. A. Steele, J. Phys. Chem. **88**, 6514 (1984).
[55]R. W. Impey, P. A. Madden, and I. R. McDonald, Mol. Phys. **46**, 513 (1982).
[56]F. H. Stillinger and T. A. Weber, Science **225**, 983 (1984).
[57]R. M. Stratt, Acc. Chem. Res. **28**, 201 (1995).
[58]T. Keyes, J. Phys. Chem. A **101**, 2921 (1997).
[59]M. Buchner, B. M. Ladanyi, and R. M. Stratt, J. Chem. Phys. **97**, 8522 (1992).
[60]R. M. Stratt and M. Cho, J. Chem. Phys. **100**, 6700 (1994).
[61]B. M. Ladanyi and R. M. Stratt, J. Phys. Chem. **99**, 2502 (1995).
[62]B. M. Ladanyi and S. Klein, J. Chem. Phys. **105**, 1552 (1996).
[63]B. M. Ladanyi and R. M. Stratt, J. Phys. Chem. A **102**, 1068 (1998).
[64]M. Cho, G. R. Fleming, S. Saito, I. Ohmine, and R. M. Stratt, J. Chem. Phys. **100**, 6672 (1994).
[65]S. L. Chang, T. M. Wu, and C. Y. Mou, J. Chem. Phys. **121**, 3605 (2004).
[66]K. H. Tsai and T. M. Wu, Chem. Phys. Lett. **417**, 389 (2006).
[67]Y. C. Chen, P. H. Tang, and T. M. Wu, J. Chem. Phys. **139**, 204505 (2013).
[68]H. Goldstein, *Classical Mechanics*, 2nd ed. (Addison-Wesley, Boston, 1980).
[69]R. Kubo, M. Toda, and N. Hashitsume, *Statistical Physics II, Nonequilibrium Statistical Mechanics* (Springer-Verlag, New York, 1982).
[70]For a SPC/E water molecule, the moments of inertia with respect to the x' and y' axes are given as $I_{||} = I_x \cos^2\theta + I_y \sin^2\theta$ and $I_\perp = I_x \sin^2\theta + I_y \cos^2\theta$, respectively, where I_x and I_y are the moments of inertial with respect to the principal x and y axes.
[71]Y. Wan and R. M. Stratt, J. Chem. Phys. **100**, 5123 (1994).
[72]R. E. Larsen, E. F. David, G. Goodyear, and R. M. Stratt, J. Chem. Phys. **107**, 524 (1997).
[73]J. Jang and R. M. Stratt, J. Chem. Phys. **112**, 7524 (2000).
[74]J. Jang and R. M. Stratt, J. Chem. Phys. **112**, 7538 (2000).
[75]J. Jang and R. M. Stratt, J. Chem. Phys. **113**, 5901 (2000).
[76]T. M. Wu and R. F. Loring, J. Chem. Phys. **99**, 8936 (1993).
[77]P. H. Tang, T. M. Wu, T. W. Yen, S. K. Lai, and P. J. Hsu, J. Chem. Phys. **135**, 094302 (2011).
[78]S. Saito and I. Ohmine, J. Chem. Phys. **108**, 240 (1998).
[79]J. L. Finney, Proc. R. Soc. London, Ser. A. **319**, 479 (1970).
[80]Y. L. Yeh and C. Y. Mou, J. Phys. Chem. B **103**, 3699 (1999).
[81]With $\alpha \approx 64.8^\circ$, $\cos^2\alpha \approx 0.182$, and $\sin^2\alpha \approx 0.818$. With $\beta \approx 43.3^\circ$, $\cos^2\beta \approx 0.530$, and $\sin^2\beta \approx 0.470$.
[82]The spectral maxima of $D_{||}^{INM,s}(\omega)$, $D_{\perp}^{INM,s}(\omega)$, and $D_z^{INM,s}(\omega)$ were located near 790, 560, and 520 cm^{-1}, respectively, and their spectral widths were approximately 600, 650, and 380 cm^{-1}, respectively. The rotational stable-INM spectrum of an axis is broader than the AVAF power spectrum of the axis since there is no motional narrowing effect in the INM theory.[67]
[83]A. J. Leggett, S. Chakravarty, A. T. Dorsey, M. P. A. Fisher, A. Garg, and W. Zwerger, Rev. Mod. Phys. **59**, 1 (1987).
[84]U. Weiss, *Quantum Dissipative Systems*, 2nd ed. (World Scientific, London, 2001).
[85]T. M. Wu, D. W. Brown, and K. Lindenberg, Chem. Phys. **146**, 445 (1990).
[86]T. M. Wu, D. W. Brown, and K. Lindenberg, Phys. Rev. B **47**, 13854 (1993).
[87]L. M. Svishchev and P. G. Kusalik, J. Phys. Chem. **98**, 728 (1994).
[88]T. M. Wu and S. F. Tsay, J. Chem. Phys. **105**, 9281 (1996).
[89]T. M. Wu, S. L. Chang, S. F. Tsay, and K. H. Tsai, J. Non-Cryst. Solids **352**, 4615 (2006).
[90]The average frequency of $D_{\mu\xi}^{INM,s}(\omega)$ was evaluated using the formula $\omega_{\mu\xi} = \int_0^\infty \omega D_{\mu\xi}^{INM,s}(\omega) d\omega$.